X-Ray radiation (XST)

Anfangerpraktikum Teil III, Physik Department, TUM

Berke Mert
Matr. 03738893

Jedd Page
Matr. 03746102

21. June 2023

Contents

1 Introduction **2**

2 Theoretical foundation **2**
2.1 producing x-rays with an x-ray tube . . . 2
2.2 Absorption of X-Rays . . . 3
2.3 Measuring x-ray radiation using a Geiger-Müller counter . . . 4
2.4 Dead time of the detector . . . 5
2.5 x-ray diffraction on crystal lattices . . . 5

3 Experimental procedure **6**

4 Evaluation & results **7**
4.1 Determination of angle uncertainty . . . 7
4.2 Spectrum of Molybdenum X-Ray tube . . . 7
4.3 Transmission and Absorption curves of a Zirconium foil . . . 8
4.4 Lattice constant of the LiF crystal . . . 9
4.5 Determination of dead time . . . 10
4.6 Determination of the Planck constant . . . 11

5 Short questions **12**

6 Appendix **13**
6.1 Error analysis . . . 13
6.1.1 Weighted arithmetic mean . . . 13
6.1.2 Gaussian Error Propagation . . . 13
6.2 Tables . . . 13
6.3 Literature . . . 14

1 Introduction

X-ray radiation has many application, ranging from medicine to quality control in mass production. In the following experiment we observe some of the properties of x-ray radiation. We will take a look at the diffraction of x-rays on single crystals, the absorption behaviour on zirconium foil, the dead time of a Geiger-Müller counter, a typical measuring device for x-rays and finally we will determine Planck's constant.

2 Theoretical foundation

X-rays are the electromagnetic waves produced by the breaking of energetic electron in the electron cloud of an atom. The following equation gives us the relation of between the wavelength and the energy of a photon.

$$E = h \cdot \nu = h \cdot \frac{c}{\lambda} \tag{1}$$

Where h is planck's constant. [1]

2.1 producing x-rays with an x-ray tube

X-rays can be produced with an x-ray tube. A schematic diagram of one such device can be seen in figure 1

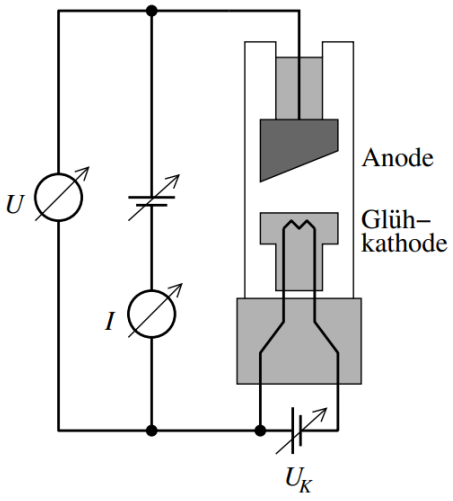

Figure 1: Schematic representation of an x-ray tube.

An x-ray tube works by accelerating electrons emitted through heat emission in the cathode. The accelerating voltage is high, typically in the range of a few 10kV. This ensures the electrons have sufficient energy when hitting the anode. The electrons entering the anode then produce x-rays via two different processes namely bremsstrahlung and scattering processes. The x-rays produced via bremsstrahlung have a continuous spectrum. We also see a line spectrum from the characteristic radiation. Electrons enter the anode with the the energy $E = e \cdot U$. If they give up all their energy in a single process they emit a photon with wavelength $\lambda_0 = \frac{h \cdot c}{e \cdot U}$ Shorter wavelengths cannot be created. This explains the starting position of the emission spectrum, which can be seen in figure 2.

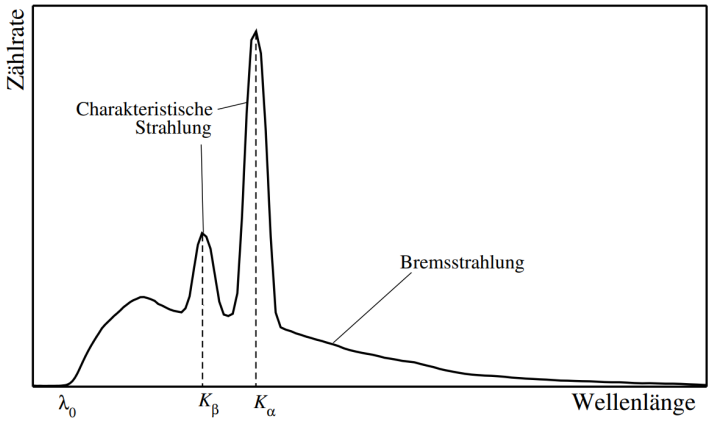

Figure 2: The typical emission spectrum of an x-ray tube.

The bremsstrahlung curve then increases to a maximum, where after it decreases asymptotically to zero. The characteristic peaks, which can be seen clearly in the emission spectrum, are caused by the ionisation of atoms through electron impacts and the following return of the atom to its ground state. The return of the atom to its ground state creates a photon, corresponding to the the energy levels of the atom, as such the emitted spectrum is a line spectrum and unique to the specific atom. An example energy level diagram ca be seen in figure 3.

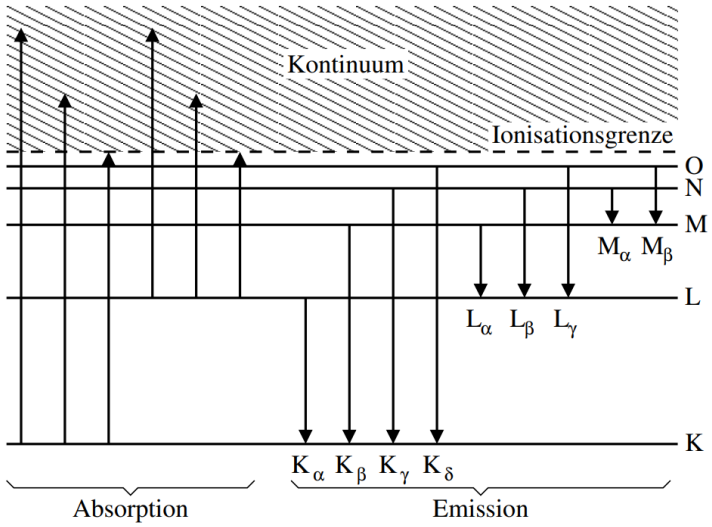

Figure 3: Schematic diagram of the energy levels of atomic transitions.

2.2 Absorption of X-Rays

When an electromagnetic wave moves through an absorbing material, also called an absorber, it loses energy through interaction with material. This energy absorption is due to three processes, namely: the photo

effect, the Compton effect and elastic scattering. The loss of intensity is given by

$$I(d) = I_0 \cdot \exp(-\mu d) \tag{2}$$

Where I_0 is intensity before the absorber, d the distance the wave has travelled in the medium and μ a material dependent parameter called the absorption coefficient. The absorption coefficient has the following proportionality

$$\mu \propto Z^5 \cdot \lambda^3 \tag{3}$$

with the Z charge number of the atoms in the absorber material. The dependence of the absorption coefficient on the wavelength can be seen in figure

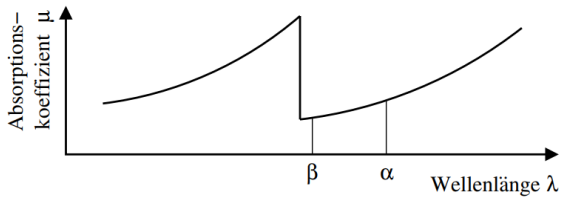

Figure 4: qualitative Wavelength dependence of the Absorption coefficient μ.

. We can see sudden drops in the absorption coefficient at certain wavelengths, these are called absorption edges. As the wavelength decreases (energy increases), more the energy levels of the lower atom orbitals are reached and are thus available for photon interaction. Most experimental methods measure the transmission of a sample rather than its absorption. This is done by measuring the starting intensity of the radiation and measuring the intensity after the sample. The transmission is then given by

$$T(\lambda) = \frac{I(\lambda)}{I_0(\lambda)}, \tag{4}$$

From the transmission we can also calculate the absorption.

$$R(\lambda) = 1 - T(\lambda), \tag{5}$$

where I is the intensity in the absorber material and I_0 is the intensity without the absorber material.

2.3 Measuring x-ray radiation using a Geiger-Müller counter

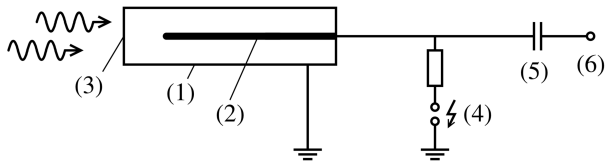

Figure 5: Schematic representation of the Geiger-Müller counter. With the following components: (1) counter body, (2) wire, (3) entry window, (4) high voltage, (5) capacitor, (6) data port.

The Geiger-Müller counter is widely used to measure radiation. A schematic representation of a Geiger-Müller counter can be seen in figure 5 The Geiger-Müller counter works through the ionisation of gas molecules by incoming x-ray radiation. The counter's electric field then pulls the ions to the electrodes, where a current can be measured and processed further.

2.4 Dead time of the detector

Immediately after the measurement of a particle many detectors need a certain amount of time before they can measure another particle. This dead time τ means that all particles are counted, which has to be accounted for. In the case of a paralyzable detector, a particle hitting the detector during dead time causes another dead time to start and as such increases the total dead time. We can calculate the real hits from the measured hits for a paralyzable detector using

$$R_z = R \cdot \exp(-R \cdot \tau) \tag{6}$$

2.5 x-ray diffraction on crystal lattices

In order to make wavelength specific measurements we use lattices, in our case crystal lattices, as they have a sufficiently small lattice constant to allow the interference of x-ray radiation. This interference can be used in Bragg scattering in order to filter for different wavelengths as the constructive interference condition is wavelength dependent. We see this in the Bragg condition

$$n \cdot \lambda = 2d \cdot \sin \Theta_n \; n = 1, 2, 3... \tag{7}$$

A goniometer in the x-ray spectrometer makes a $\Theta - 2\Theta$.

3 Experimental procedure

The experiment was done on the educational x-ray machine (LD-didactic 554 81) with an molybdenum anode, all parameters were set directly on the machine
The first measurement done was the measurement of the x-ray tube's emission spectrum. To this end a single NaCl crystal was placed on the sample holder. The voltage was set to $U = 35\text{kV}$ with an emission current of $I = 0.8\text{mA}$. The angle steps were set to $\Delta\beta = 0.1°$ with an exposure time of $\Delta t = 1\text{s}$. The measurement was done within the angle interval $2° - 25°$.
For the second measurement, the absorption in a zirkonium foil, the 0.05mm thick foil is placed over the detector and only the angle interval was changed to $4° - 10°$.
For measurement of the angle precision the crystal is rotated by 180° and the measurement repeated once again in the interval $2° - 10°$.
Thereafter the NaCl crystal is replace with a LiF crystal and the measurement repeated again in the interval $2° - 25°$.
the goal of the second to last measurement is to determine the intensity dependence of the emission spectrum, for this the spectrum is measured for different currents in the interval $I = 0.1 - 1.0\text{mA}$ in steps of 0.1mA. The voltage is increased to 25kV and the exposure time to 4s. The measurement interval is $8° - 11°$.
The last measurement of the experiment is used to determine Planck's constant and the. The measurement parameters can be seen in table ...

4 Evaluation & results

All K_α^n-, K_β^n-lines, were found using the the peak finding algorithm of the measuring software "X-Ray" used in the experiment. It has the added benefit of returning the uncertainty of the angle. The uncertainty calculations can be found in the error analysis chapter 6.1.

4.1 Determination of angle uncertainty

First, the overlapping peaks and their uncertainty are determined, where the uncertainty of each peak is given by the max upper and lower bounds of the overlapping peaks. To approximate the angle uncertainty, the bigger of the two uncertainty is taken and added to the statistical uncertainty. This result in an overall angle uncertainty of,

$$u(\theta) \approx 0.05^\circ + 0.04^\circ = 0.09^\circ. \tag{8}$$

Figure 6 summarises our procedure and results.

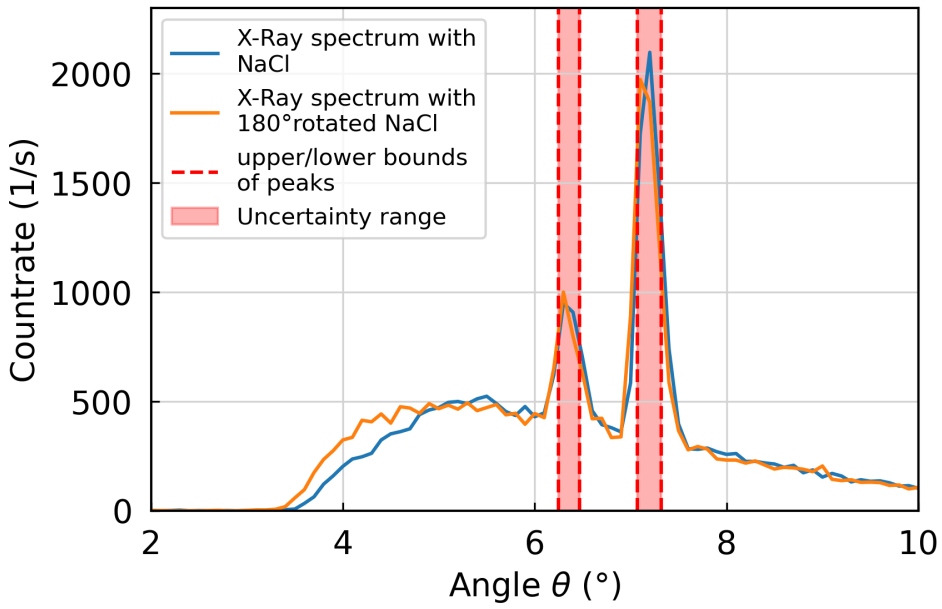

Figure 6: Determination of angle uncertainty of the NaCl crystal. The orange X-Ray spectrum is measured by rotating the crystal by 180° around the normal axis of the sample desk. The wider of the two uncertainty ranges makes up our systematic uncertainty on the angle.

4.2 Spectrum of Molybdenum X-Ray tube

Figure 7 shows the full X-Ray spectrum of a Molybdenum anode with a NaCl crystal between the angles 2° to 25°. From this spectrum, all the K_α^n-, K_β^n-lines up to third order can be determined. Now, equations (7) and (1) can be used to calculate the wave length and energy of the light, which can found in table 1.
Finally, the the weighted mean average of the wave lengths and energy can be taken for the K_α and K_β emission lines, which results in $\lambda_\alpha = (70.81 \pm 0.16)$ pm and $\lambda_\beta = (62.90 \pm 0.16)$ pm for the wave lengths, and

$E_\alpha = (17.51 \pm 0.04)\,\mathrm{keV}$ and $E_\beta = (19.71 \pm 0.05)\,\mathrm{keV}$ for the energies. These results are well within the uncertainty range with the literature values $E_{lit,\alpha} = 17.48\,\mathrm{keV}$ and $E_{lit,\beta} = 19.61\,\mathrm{keV}$ and therefor satisfactory [2].

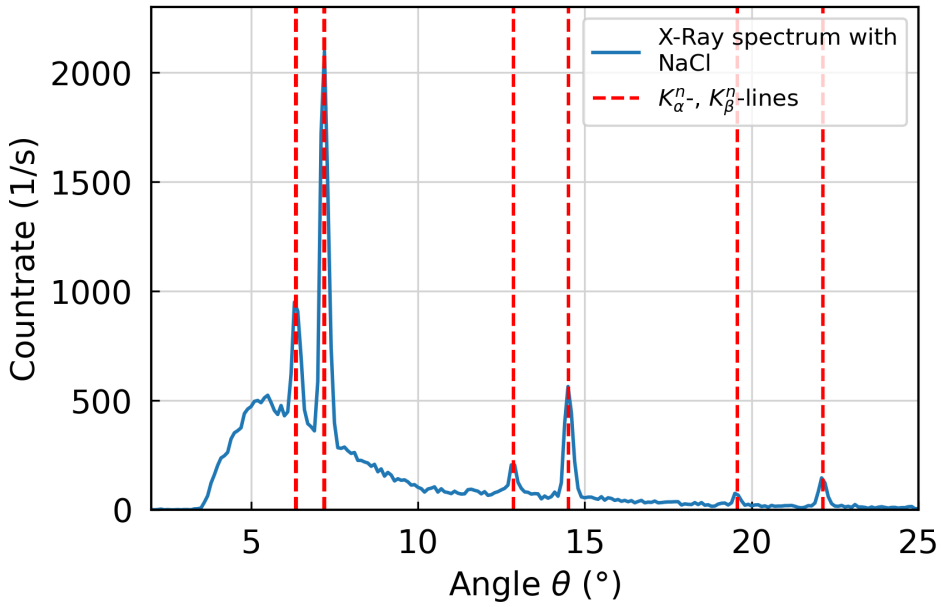

Figure 7: X-Ray spectrum of NaCl crystal with K^n_α-, K^n_β-lines up to third order.

4.3 Transmission and Absorption curves of a Zirconium foil

To determine the Transmission and Absorption curves of a Zirconium foil, first, the measured angle of the spectra with and without the Zr foil is converted using equation 7. Then, the fact we can use the fact that the count rate is directly proportional to the intensity and determine the Transmission and Absorption curves can be calculated using equations (4), (5), which results in figure 8.
From this figure, it can be seen that the Transmission increases at certain wave length range marked in grey. The average of the lower and upper bounds of the so-called absorption edge results in $\lambda_{exp} = (68.0 \pm 1.0)\,\mathrm{pm}$ (uncertainty is given by difference of the average and lower bound), and therefor in $E_{exp} = (18.23 \pm 0.26)\,\mathrm{keV}$ using equation (1). This result is overlapping with the literature value $\lambda_{lit} = 68.88\,\mathrm{pm}$ and is therefor satisfactory [3].

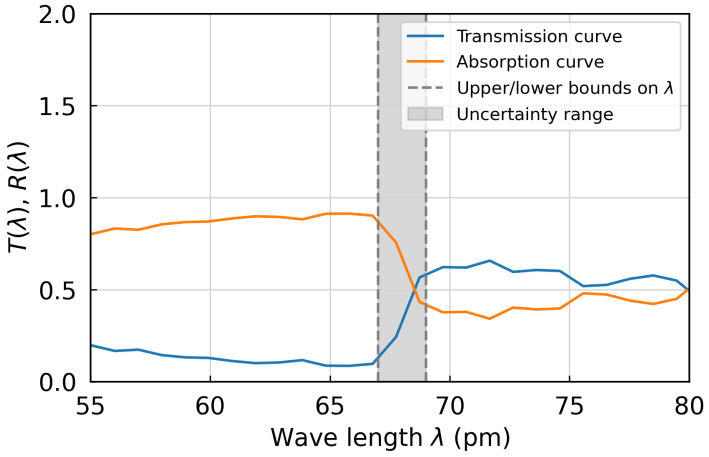

Figure 8: Transmission and Absorption curves of a Zirconium foil.

4.4 Lattice constant of the LiF crystal

The X-Ray spectrum of a Molybdenum anode with a LiF crystal with K_α^n-, K_β^n-lines up to second order is shown in figure 9. From the angle positions of the peaks, the lattice constants can be calculated using Bragg condition (7),

$$d = \frac{\lambda \cdot n}{2 \cdot \sin\theta}, \qquad a = 2 \cdot d,$$

where wave lengths λ are taken from chapter 4.2.
This results in the values in table 2, which are used to determine the weighted mean average $d_{exp} = (204.98 \pm 0.66)\,\text{pm}$, $a_{exp} = (409.96 \pm 1.32)\,\text{pm}$. This result is very close to the literature value of the lattice constant of 403 pm for a LiF crystal and therefore satisfactory[4].

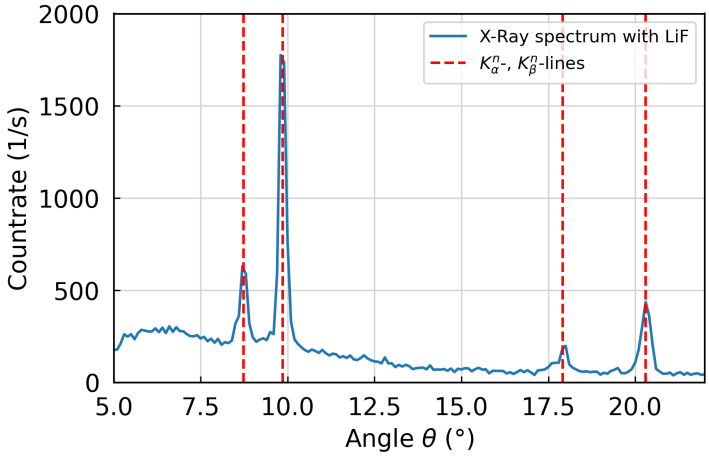

Figure 9: X-Ray spectrum of LiF crystal with K_α^n-, K_β^n-lines up to second order.

4.5 Determination of dead time

Figure 10 shows X-Ray spectrum of Molybdenum anode for different emission current, which shows a relationship between the emission current and the count rate in the form of,

$$R_Z(I) = R_0 \cdot \exp\left(-R_0\tau\right) = r \cdot I \cdot \exp\left(-r \cdot I \cdot \tau\right),$$

assuming $R_0 \propto I$.
Here, the maxima of the K_α^1 lines are gathered and assigned the respective emission current, plotted in figure 11, and then fitted with the linear function, which results in $\tau = (77.20 \pm 4.64)\,\mu$s and $r = (2738.51 \pm 33.02)\,$cps/mA.

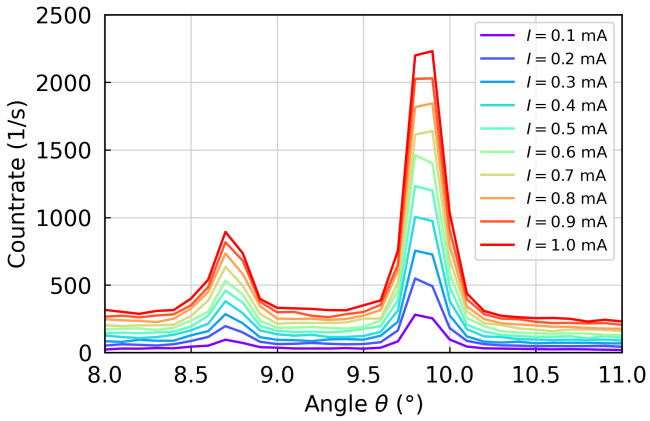

Figure 10: X-Ray spectrum of a LiF crystal for different emission currents. The right count rates of the K_α^1 lines one the right are used for further evaluation.

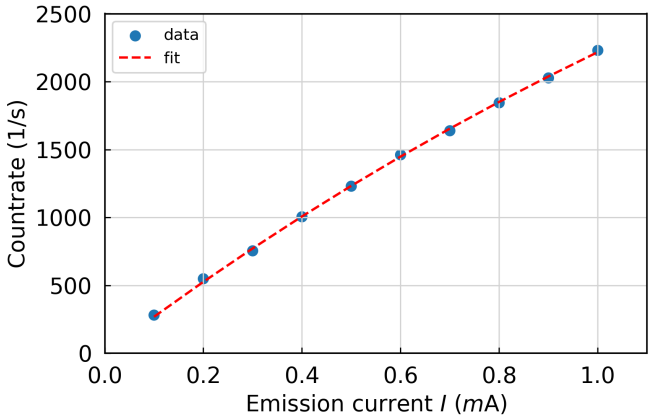

Figure 11: K_α^1 count rate vs. emission current I. A fit of the data points reveals the dead time τ of the detector.

4.6 Determination of the Planck constant

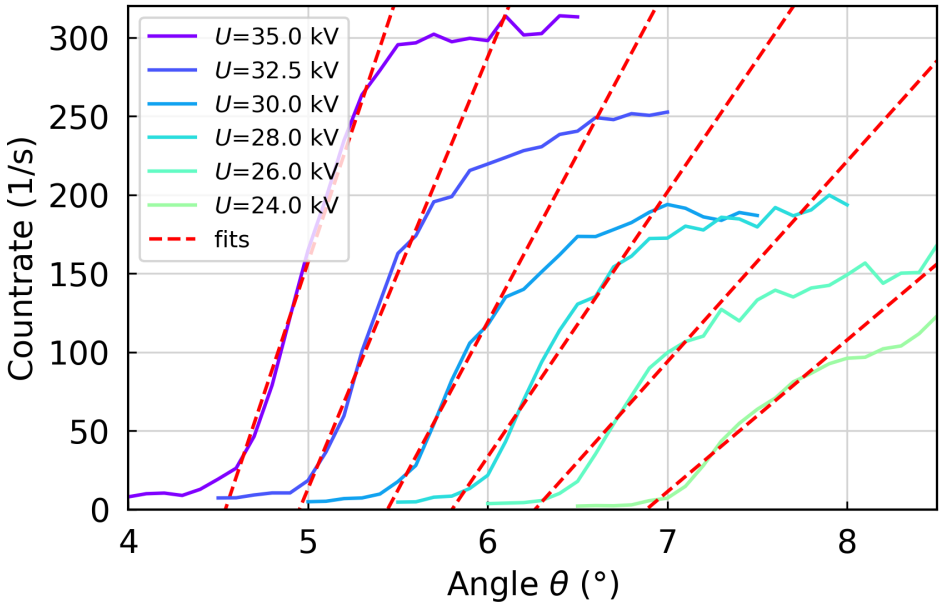

Figure 12: X-Ray spectra of a LiF crystal for different voltages near the cut-off angle θ_0.

With the last set of measurements the cut-off wavelength, λ_0, of the Bremsstrahlung is determined. Figure 12 shows the Bremsstrahlung near the cut-off angle for different acceleration voltages.
The cut-off angle is determined by first performing fit on the part of the spectra with a large derivative with a linear function,

$$N(\theta) = a \cdot \theta + b,$$

and secondly, finding the roots of the function with a root searching algorithm, which can also be converted to a cut-off wave length using Bragg's condition (7).
Lastly, Planck's constant can be determined using equation (1) by solving for the constant,

$$h = \frac{\lambda_0 \cdot e \cdot U}{c}.$$

This results in the values in table 3. The weighted average of the measured results is
$h_{exp} = (6.07 \pm 0.04) \cdot 10^{-34}$Js, which only deviates by 9% of the literature value $h_{lit} = 6.63 \cdot 10^{-34}$Js.

5 Short questions

1. **Assuming sufficient intensity what is the maximum achievable reflection angle of the K_α line for the two used crystals? What are the orders of these maxima**
   The literature value of the K_α line is $\lambda = 71.08$pm[5]. Using the Bragg-condition 7 and the condition $\sin \leq 1$ we get the
   $$n \leq \frac{2 \cdot d}{\lambda} \tag{9}$$
   With the lattice constants of 282.01 pm and (204.98 ± 1.32) pm for the NaCl and the LiF crystal respectively. we get the the orders $n_{NaCl} = 7$ and $n_{LiF} = 5$. Now it is possible to calculate the maximum reflection angle using the Bragg Condition 7
   $$\Theta = \arcsin \frac{n \cdot \lambda}{2 \cdot d} \tag{10}$$
   We get $\Theta_{NaCl} =$ and $\Theta_{LiF} =$

2. **How can one determine the energy of the L_α line using the measured data?**
   The energy of the L_α transition can be calculated with
   $$E_{L,\alpha} = E_{K,\beta} - E_{K,\alpha} \tag{11}$$
   This is due to the fact that the energy of the L_α line is given by the energy difference between the M and L shells and the K_α or the L_β lines have energies corresponding to the transitions between shells L or M to K. Using the literature values $E_{K,\beta} = 19,60$keV and $E_{K,\alpha} = 17,44$keV we get $E_{L,\alpha} = 2.16$keV.

6 Appendix

6.1 Error analysis

6.1.1 Weighted arithmetic mean

To find the mean of multiple values, that have different uncertainties, the weighted arithmetic mean

$$\frac{\sum_{i=1}^{n} w_i \cdot x_i}{\sum_{i=1}^{n} w_i} \tag{12}$$

was used, where w_i are the weights of the different data elements and are given by

$$w_i = \frac{1}{u^2(x_i)}. \tag{13}$$

$u(x_i)$ describe the errors of the different values. To find the uncertainty of the weighted mean, the inner and outer uncertainties are compared. The inner uncertainty is given by

$$u_{int}(\bar{x}) = \sqrt{\frac{1}{\sum_{i=1}^{n} w_i}} \tag{14}$$

and the outer uncertainty by

$$u_{ext}(\bar{x}) = \sqrt{\frac{\sum_{i=1}^{n}(w_i \cdot (x_i - \bar{x})^2)}{(n-1) \cdot \sum_{i=1}^{n} w_i}}. \tag{15}$$

Of the two found uncertainties, the bigger one is used [6].

6.1.2 Gaussian Error Propagation

For calculations using experimental values with uncertainties the Gaussian formula for error propagation

$$u(\bar{g}) = \sqrt{\sum_{i=1}^{N} \left(\frac{\partial g}{\partial x_i}\right)^2 u^2(\bar{x_i})}, \tag{16}$$

was used [6].

6.2 Tables

Table 1: Angle, wave length and energy of K_α^n-, K_β^n-emission lines up to third order with molybdenium anode.

Line	θ (°)	λ (pm)	E (peV)
K_β^1	6.36 ± 0.11	62.50 ± 0.63	19.84 ± 0.19
K_β^2	12.87 ± 0.08	62.81 ± 0.31	19.73 ± 0.09
K_β^3	19.57 ± 0.07	62.97 ± 0.20	19.68 ± 0.06
K_α^1	7.21 ± 0.11	70.78 ± 0.62	17.51 ± 0.15
K_α^2	14.52 ± 0.11	70.70 ± 0.30	17.53 ± 0.07
K_α^3	22.14 ± 0.09	70.85 ± 0.19	17.49 ± 0.04

Table 2: Angle and lattice constants K_α^n-, K_β^n-emission lines up to second order.

Line	θ (°)	a (pm)	d (pm)
K_β^1	8.73 ± 0.14	413.51 ± 2.80	206.75 ± 1.40
K_β^2	17.9 ± 0.08	408.20 ± 1.77	204.10 ± 0.88
K_α^1	9.86 ± 0.09	414.42 ± 4.12	207.21 ± 2.06
K_α^2	20.3 ± 0.14	409.29 ± 2.05	204.64 ± 1.02

Table 3: Cut-off angle, wave length and experimentally determined Planck constant.

U (kV)	θ_0 (°)	λ_0 (pm)	h (10^{-34} Js)
35.0 ± 0.5	4.53 ± 0.50	31.88 ± 0.35	5.96 ± 0.09
32.5 ± 0.5	4.95 ± 0.50	34.76 ± 0.35	6.03 ± 0.09
30.0 ± 0.5	5.44 ± 0.50	38.20 ± 0.35	6.12 ± 0.10
28.0 ± 0.5	5.80 ± 0.50	40.71 ± 0.35	6.09 ± 0.11
26.0 ± 0.5	6.26 ± 0.50	43.93 ± 0.35	6.10 ± 0.12
24.0 ± 0.5	6.88 ± 0.50	48.26 ± 0.35	6.19 ± 0.13

6.3 Literature

References

[1] Physics department TUM. Röntgenstrahlung (XST). `https://www.ph.tum.de/academics/org/labs/ap/ap3/XST.pdf`, 2023. last visited 2.7.2023.

[2] Lawrence Berkeley National Laboratory. *Photon energies, in electron volts, of principal K-, L-, and M-shell emission lines.* LBNL, `https://xdb.lbl.gov/Section1/Table_1-2.pdf`. Last visited 5.7.2023.

[3] Author unknown. *Absorption Edge of Zr.* Unknown, `https://www.ld-didactic.de/literatur/hb/d/p6/p6335_d.pdf`. Last visited 5.7.2023.

[4] Author unknown. *Lattice Crystall properties.* Alineason Materials and Technologies, `https://www.alineason.com/produkt/lithiumfluorid/`. Last visited 5.7.2023.

[5] LD Didactic GmbH. Feinstruktur der charakteristischen röntgenstrahlung einer molybdän-anode. https://www.ld-didactic.de/literatur/hb/d/p6/p6361$_d$*.pdf*, 2023. *lastvisited*11.07.2023.

[6] Physics department TUM. Hinweise zur Beurteilung von Messungen, Messergebnissen und Messunsicherheiten (ABW). `https://www.ph.tum.de/academics/org/labs/ap/org/ABW.pdf`, 20xx. last visited 5.5.2021.